Extreme Mechanics Letters 37 (2020) 100688

Contents lists available at ScienceDirect

Extreme Mechanics Letters

journal homepage: www.elsevier.com/locate/eml

Compression and buckling of microarchitectured Neovius-lattice

Diab W. Abueidda [a,1], Mohamed Elhebeary [a,1], Cheng-Shen (Andrew) Shiang [a], Rashid K. Abu Al-Rub [b], Iwona M. Jasiuk [a,*]

[a] *Department of Mechanical Science and Engineering, University of Illinois at Urbana-Champaign, 1206 West Green Street, Urbana, IL 61801-2906, USA*
[b] *Department of Aerospace Engineering, Khalifa University of Science and Technology, Abu Dhabi, United Arab Emirates*

ARTICLE INFO

Article history:
Received 11 November 2019
Received in revised form 5 February 2020
Accepted 23 March 2020
Available online 8 April 2020

Keywords:
Coating
Size effect
In-plane and out-of-plane buckling
Microlattice
Triply periodic minimal surfaces
Two-photon polymerization

ABSTRACT

New materials with enhanced properties are of high scientific and industrial interests. Microarchitectured cellular materials possess robust mechanical properties such as high strength-to-weight ratios due to their architectures and size effect appearing in metals and ceramics. In this study, we investigate the mechanical properties of a novel microlattice based on the Neovius surface, a member of the triply periodic minimal surfaces. We show that the Neovius-microlattice exhibits high uniaxial modulus, energy absorption, and strength due to its architecture, which is free of self-intersecting elements. The polymeric Neovius-microlattice deforms locally by two mechanisms: buckling and plastic yielding, while the brittle fracture is not observed. Also, we show that the mechanical properties of the Neovius-microlattice can be enhanced further by coating it with a ceramic (alumina) layer. Additionally, the nature of instability in these architectured materials (at the micro-scale, microns in dimensions) is explored through experiments and computational modeling. The two primary instability mechanisms, out-of-plane and in-plane buckling, in cellular materials, are distinguished. Such a study can pave the path for designing cellular materials that are stiff, strong, light, and buckling-resistant.

1. Introduction

There are many wide and varied goals when it comes to materials' design, ranging from mechanical properties to even aesthetic pleasantness. In the last decade, the development of new materials with exceptional mechanical, electrical, optical, and corrosion-resistance properties attracted many researchers. For example, producing lighter yet stronger materials has always been, and continues to be a primary focus for many industrial applications. A lighter material with comparable mechanical properties to those of current materials would translate to a higher fuel economy for the transportation sector, higher efficiencies for the energy sector, and open up new possibilities for the construction industry [1–5]. To achieve such a goal, one can create new architectures using existing materials [1,6]. One class of such candidate materials are periodically repeating architectured cellular materials. Researchers have shown that such architectured materials can be designed to have more desirable properties than the bulk material [7–11]. Furthermore, such designs enable the finetuning of mechanical properties to suit different needs better [9,10,12–17], or even introduce unusual behaviors such as negative Poisson's ratios [18].

Another significant advantage of architectured materials is their ability to benefit from the favorable size effects of bulk materials. Such effects can be observed in micro/nanoscale thin films of metal with grain sizes of 10∼20 nm [11,19–24], for example. These micro-architectured metal designs can be fabricated by depositing thin metal films onto additively manufactured polymer scaffolds [11,13]. Torrents et al. [25] created, tested, and characterized nickel-based microlattices spanning three different length scales. For ultra-low densities (<0.1%), the lattices interestingly exhibited a full recovery after applying an engineering strain as high as 50%. For higher densities, plastic deformation was induced. For such lattices, optical and electron microscopy imaging concluded that the deformation was primarily localized at the nodes of the lattices. Also, ceramics are another type of material that has size effects beneficially at the nano-scale [20,26–30]. Micro-architectured design of ceramic composites can be found frequently in nature, such as in bones and nacre [6,26,31,32]. In addition to the use of metallic and ceramic coatings for micro-architectured cellular materials to improve their mechanical properties, one can enhance the mechanical properties by improving the properties of the underlying polymer itself. Schroer et al. [33] showed that appropriate annealing treatments could significantly increase the mechanical properties of the base

* Corresponding author.
E-mail address: ijasiuk@illinois.edu (I.M. Jasiuk).
[1] D.A. and M.E. contributed equally to this work.

https://doi.org/10.1016/j.eml.2020.100688
2352-4316/

polymer. Micro-/nano-lattices either performed comparably to macro counterparts or had more desirable mechanical properties [28,33–37]. Also, introducing hierarchy, in which unit cells span several length scales, into architected materials leads to a unique combination of properties such as ultralightweight, recoverability, and near-linear scaling of stiffness and strength with density [38].

There are different ways to manufacture micro-scale architectured samples (microns in dimensions). To fabricate structures at the micro-scale, a new and growing technology called a two-photon polymerization (2PP) is often employed [8,27,33–35,39–46]. Also, researchers have successfully used a large area projection microstereolithography (LAPμSL) [20,47–49], self-propagating photopolymer waveguide (SPPW) [11,50,51], and continuous liquid interface production (CLIP) [49,52] to fabricate microarchitectured materials. Many studies have performed *in-situ* testing for micro-fabricated materials obtained using these different fabrication techniques [10,27,42,53,54]. Most of the mechanical testing is performed inside a scanning electron microscope (SEM) chamber to allow both quantitative and qualitative characterization of deformation mechanisms. Also, nanoindentation is widely implemented for micro-compression testing [13,36]. As for tensile testing, both nanoindenters with custom grips [55] and micro-load frames are employed [56].

Generally, cellular materials fail when compressive loads are increased due to either material plastic yielding, brittle fracture, or buckling. Bulk materials encounter elastic structural instability emerging as out-of-plane deformation. In contrast, cellular materials experience an out-of-plane buckling as well as an in-plane failure (fracture, yielding, or buckling). Unlike the out-of-plane buckling, the in-plane buckling significantly depends on the materials' architecture [57–59]. In the literature, out-of-plane and in-plane bucklings are sometimes referred to as global and local bucklings, respectively. The buckling of cellular materials is an active area of research, and it was not extensively studied so far [60–62]. The distinction between the global and local buckling of micro-architectured materials is scarce. However, reasonable assumptions can be drawn from the buckling of architectured materials at the macro-scale (whole specimen) or those that have unit cells with dimensions in millimeters. He et al. [62] demonstrated that by altering the thickness ratios between cell size and different sections of the cell wall, it is possible to control the buckling mode of the structure. Additionally, Niknam et al. [61] showed that cellular plates have a 20% higher buckling load than homogeneous plates for specific geometries. Furthermore, they concluded that slenderness ratio, relative density ρ_r, and cell topology are essential parameters to determine buckling behaviors such as in-plane or out-of-plane buckling mode shapes.

In this paper, the mechanical response of one member of the triply periodic minimal surfaces (TPMS) family under compression is studied at the micro-scale. TPMS are well-known surfaces with zero mean curvature that are characterized by local area minimizing, and such micro-architectures appear in nature [63–65]. TPMS possess continuous smooth connections, free of self-intersecting elements, whether they are used to make interpenetrating phase composites [12,66,67] or cellular materials [8,68–71]. The smooth connection provides stronger mechanical properties than those of conventional strut-based architectured materials [8,66,68,71]. A comparison between TPMS and conventional architectured material designs is demonstrated by Al-Ketan et al. [71]. Feng et al. [72] showed that TPMS's smooth continuity allowed for free form T-spline skin faces, which trumped traditional sandwiched panels with lattice cores in mechanical, permeability, and energy absorption performances. Some known TPMS geometries are Schwarz Primitive, Neovius, IWP, and Gyroid, which have been studied in previous works [8,63,66,68,69,71,73–76].

This paper focuses on the TPMS Neovius microlattice (see Fig. 1). Previously, the Neovius-lattice with cell sizes on the order of a few millimeters was studied with the smallest feature sizes on the order of several hundreds of microns [70]. In this work, the Neovius-microlattices were fabricated at the micro-scale using the 3D direct laser writing (DLW) based on 2PP. The sample sizes were a few hundred microns with the smallest features of several microns. Also, the influence of coating and accompanied size effect on the mechanical properties of the Neovius-lattice was investigated, which was not explored before for the Neovius-microlattice and other sheet-like microlattices, in general. The Neovius-microlattices were subjected to compressive loading in an SEM chamber, where the deformations of the Neovius-lattice, including out-of-plane and in-plane buckling, were investigated. Such a distinction between out-of-plane and in-plane buckling is useful, as it provides insights when one is interested in designing 3D hierarchical materials. Finally, the experiments were complemented by theoretical study. Finite element analysis (FEA) was conducted to identify the dominating failure mechanisms of the Neovius-microlattice and its deformations, which are different from truss-like materials. Analytical formulations were obtained for scaling laws. This paper presents a framework for future studies on architectured materials at the micro-scale.

2. Methodology

2.1. Experimental procedures

The samples were manufactured via Nanoscribe (Nanoscribe GmbH, Eggenstein-Leopoldshafen, Germany), a technology that has already been proven highly beneficial in the fabrication of complex architectured materials at the micro-scale [8,27,33,39,42,43,77]. The Nanoscribe is a stereolithography based 3D printer that fabricates samples by polymerizing a proprietary polymer, IP-S in the case of this study, with a laser to produce the final product. Fig. 2 shows the Neovius-microlattice and illustrates the different specimen sizes and configurations used in our study.

Fig. 2a shows a Neovius-microlattice with a periodicity of $4 \times 4 \times 4$ unit cells. Such a periodicity is enough to obtain the effective properties of the Neovius-lattice [70]. Figs. 2b and 2c show zoomed in images of the Neovius-microlattice. The density of the Neovius-microlattice is varied by controlling the sheet thickness t (minimum feature size in the case of Neovius-lattice), shown in Fig. 2c. Specimens with the cell size $l = 75$ microns (see Fig. 2a, leading to a total specimen size of 300 μm, were tested to obtain the stress–strain curves and calculate the compressive uniaxial stiffness, strength, and energy absorption. Due to the nonlinearity in the stress–strain curve, it is challenging to obtain a uniaxial modulus. Here, we calculate the uniaxial stiffness by finding the slopes of the stress–strain curve at several data points up to 5% applied strain, and then we take the average of the slopes. Strength is defined as the maximum stress achieved before any softening takes place. Energy absorption is calculated as the area under the stress–strain curve (up to 25% engineering strain). Some of the specimens were conformally coated with alumina layer using atomic layer deposition (ALD) process [78]. The coating was done via Savannah S100 (Cambridge NanoTech, Waltham, MA, USA) at 75 °C. A growth rate of 0.10 nm/cycle has been determined.

Under compressive loading, cellular materials might buckle locally (in-plane) or globally (out-of-plane). To study the buckling behavior of the Neovius-microlattices, specimens with different slenderness ratios $SR = H/T$ (see Fig. 2d–f), where H and T are the height and thickness of the specimens, respectively, as depicted in Fig. 2d, were tested and imaged. The width W and height H of the specimens were fixed, so each was 300 μm,

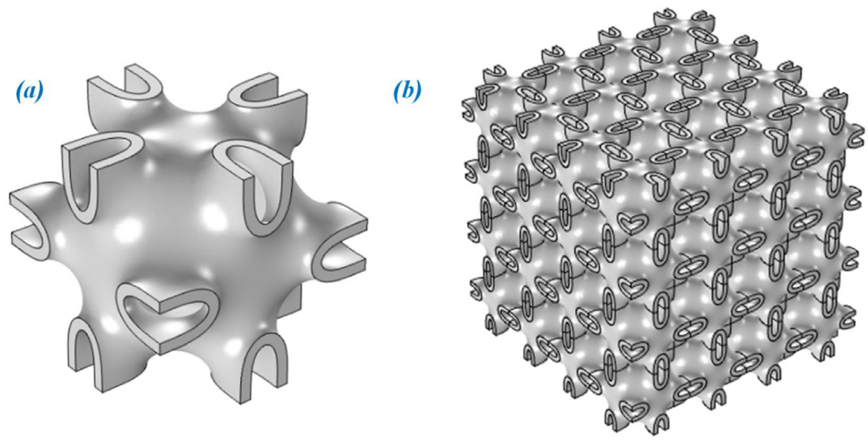

Fig. 1. CAD drawing of the Neovius-lattice: (a) one unit cell, (b) three-dimensionally periodic 64 ($4 \times 4 \times 4$) cells.

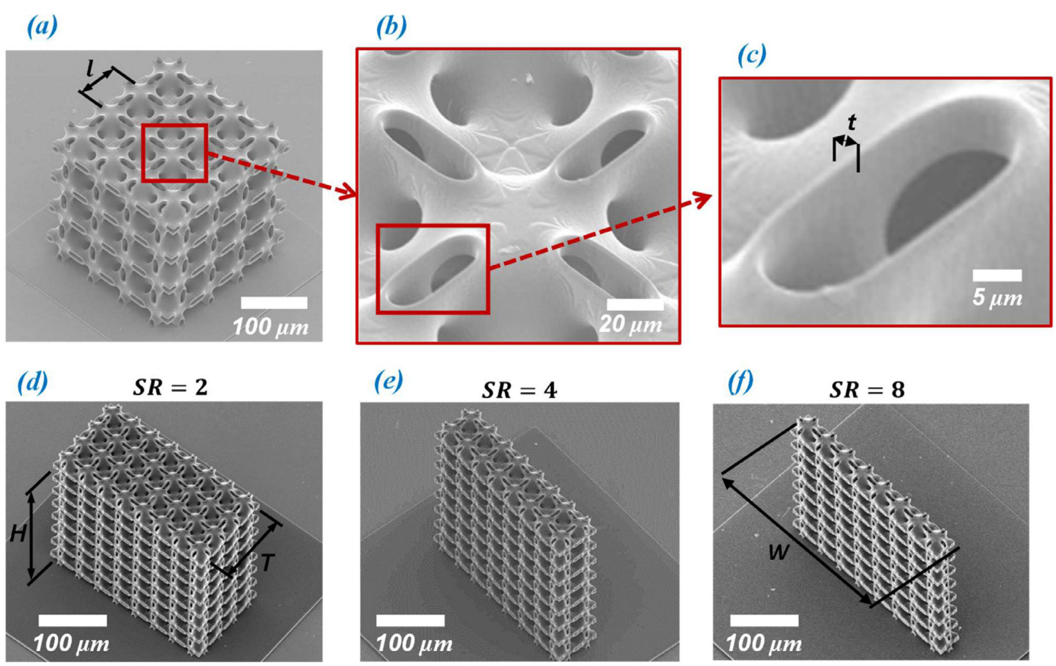

Fig. 2. SEM images of the Neovius-microlattices with 5% relative density: (a) specimen with 64 ($4 \times 4 \times 4$) unit cells used for obtaining uniaxial stiffness, compressive yield strength, and energy absorption, (b–c) zoomed in SEM images of the Neovius-microlattice, (d–f) Neovius-microlattices with different slenderness ratios $SR = H/T$, used to study buckling of microarchitectured Neovius-lattice.

while the thickness T was varied. Having a width W higher than the thickness T was vital to facilitate the imaging of the out-of-plane buckling, if any. Otherwise, imaging of the out-of-plane buckling was not guaranteed, given that the imaging was done in one direction inside the SEM chamber. The Quanta FEG 450 environmental SEM from the FEI company was utilized for this purpose. The buckling definition for attaining the buckling load adopted here was presented by Liu et al. [79] as the highest compressive load in the load–displacement curve given that the solid material has neither fractured nor yielded. A Deben Microtest stage equipped with a load cell was used to test the different configurations of the Neovius-microlattice. The effect of strain rate on the mechanical behavior is not considered in this study, and all specimens were tested with a fixed strain rate, $0.0056s^{-1}$. At least three specimens were tested for each configuration.

2.2. Finite element analysis

Finite element analyses to simulate the deformation of the Neovius-lattice were performed using COMSOL Multiphysics 5.3 software (COMSOL, Inc., Burlington, MA, USA). For the buckling analysis, eigenvalue problems were solved, assuming a linear elastic response for the base material. For the static simulations, the constitutive model was assumed to be hyperelastic (neo-Hookean)-plastic (with linear hardening) based on large deformation theory [80]. The analyses were performed using a single unit cell, where periodic boundary conditions were applied to obtain the uniaxial modulus and strength.

For global buckling analysis, a compressive force was applied at the top face with zero displacements in the lateral directions while the bottom face was fixed (zero displacements in the three Cartesian directions). One unit cell was considered to distinguish between the different failure modes taking place locally. We adopted the same boundary conditions used in the work of Valdevit et al. [81]. Compressive displacements were applied at the

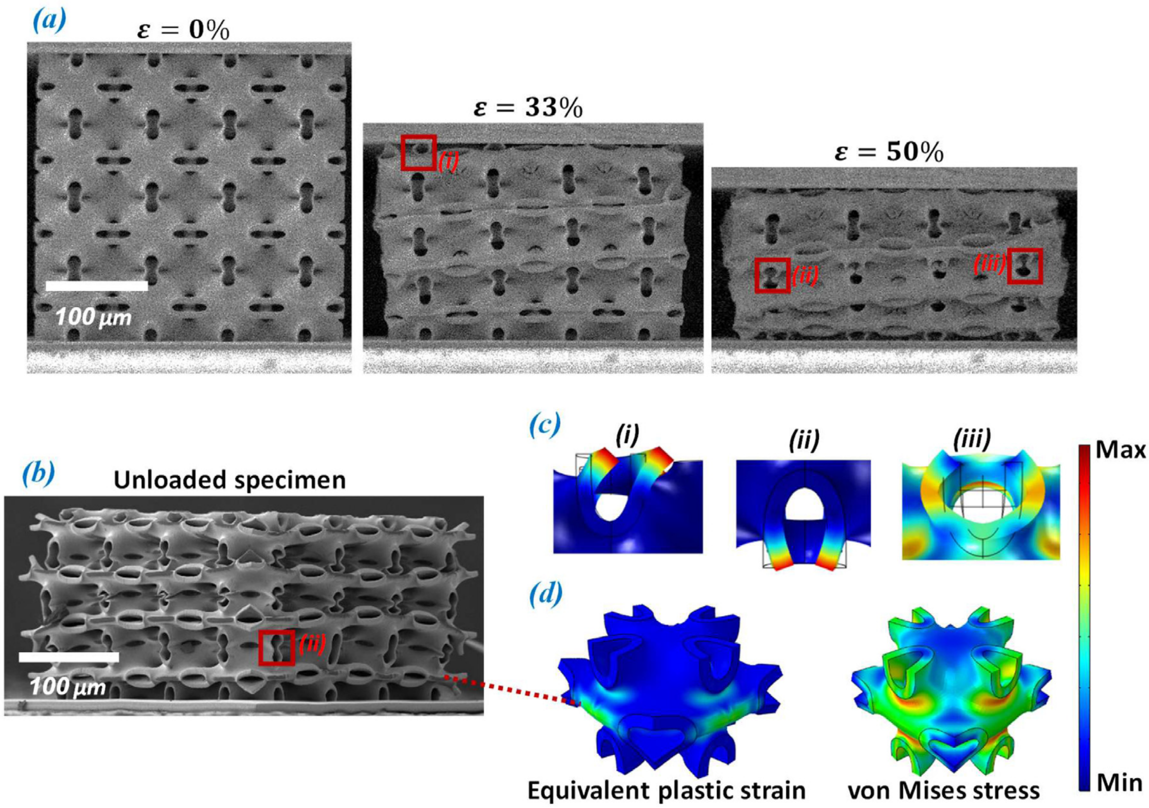

Fig. 3. Mechanical deformation of the Neovius-microlattice (ρ_r = 18%): (a) in-situ SEM images of the Neovius-microlattice at different engineering strains, (b) SEM image of the microlattice after unloading, (c) displacement obtained using the linear eigen buckling analysis, (d) equivalent plastic strain and von Mises stress obtained from hyperelastic–plastic analysis based on finite deformation theory.

top and bottom faces of the Neovius-lattice, while traction-free boundary conditions were assumed at the remaining sides.

3. Results and discussion

First, the Neovius-microlattices with $SR = 1$ at different relative densities ρ_r, defined as the ratio of the density of the cellular material to the density of the base material, were tested in compression. In-*situ* testing allowed the monitoring of the sample deformation throughout the experiment. Fig. 3a portrays an example of Neovius-microlattice loaded at three engineering strains. Fig. 3a shows that the sheet-like architecture of the Neovius-microlattice induces relatively more uniform deformations compared to those of truss-like microlattices, which mostly collapse in a layer-by-layer fashion as shown for truss-like lattices considered in [11,33,42,43]. The Neovius-microlattice maintains its structural integrity even after applying an engineering strain as high as 60%, where roughly the densification region starts (see Fig. 3b), compared to low failure strains reported in [33] (failure strains are in the range of 9%–14%) and in [42] (failure strain is up to 8%). The smooth transition between cells in the Neovius-microlattice reduces stress concentrations and enhances its overall mechanical properties. In other words, the absence of nodes/joints in the Neovius-microlattices eliminates stress concentrations and fracture in these regions, which are present in truss-like microlattices [8,33,42,82,83].

As mentioned earlier, cellular materials experience plastic yielding, brittle fracture, and/or buckling. Brittle fracture is not observed for the polymeric Neovius-microlattice under study, but this could change if the base material used was changed. Two failure mechanisms are expected for the Neovius-microlattice under investigation: local buckling and plastic yielding. To distinguish between the different deformation modes, a unit cell of the Neovius-lattice was considered, where two different analyses were performed: linear eigen buckling and hyperelastic–plastic with finite deformation to study its local buckling and plastic deformation, respectively. Fig. 3c depicts the displacement obtained from the linear eigen buckling analysis. Different buckling modes can be extracted from the buckling analysis, but only the ones observed experimentally are reported. Mainly local bucking takes place at the openings (holes) of the Neovius-lattice, while the remaining regions are buckling-free. On the other hand, Fig. 3d portrays the von Mises stress and equivalent plastic strain obtained from the hyperelastic–plastic analysis. The deformation observed in the simulation results of one unit cell matches the experimental local deformation shape captured inside the SEM. The FE analyses show that local buckling takes place at the top and bottom openings (holes) of the Neovius-lattice while plastic yielding occurs in the middle of the Neovius-lattice.

Fig. 4a depicts the stress–strain curves of the Neovius-microlattice resembling the typical response (linear region followed up by plateau and densification regions) of cellular materials. From the stress–strain curves, one can calculate the uniaxial stiffness, energy absorption, and strength, as shown in Figs. 4b and 4c. These properties are fitted by the scaling law $\phi = C\phi_s\rho_r^n$, where ϕ is the property of interest, ϕ_s is the property of the solid material used to make the cellular material, n is the fitting exponent, and C is the geometric factor. The theoretical limits for stiffness and strength of a lattice are attained when the corresponding exponent $n = 1$ and geometric factor $C = 1$, leading to a stretching-dominated response [5]. For bending-dominated cellular materials, $n = 2$ for the case of the modulus. For bending-dominated strength, $n = 2$ for elastic buckling and $n = 3/2$ for plastic buckling [5,35]. A geometric factor $C < 1$ emerges from structural defects, buckling, bending, and/or misalignments

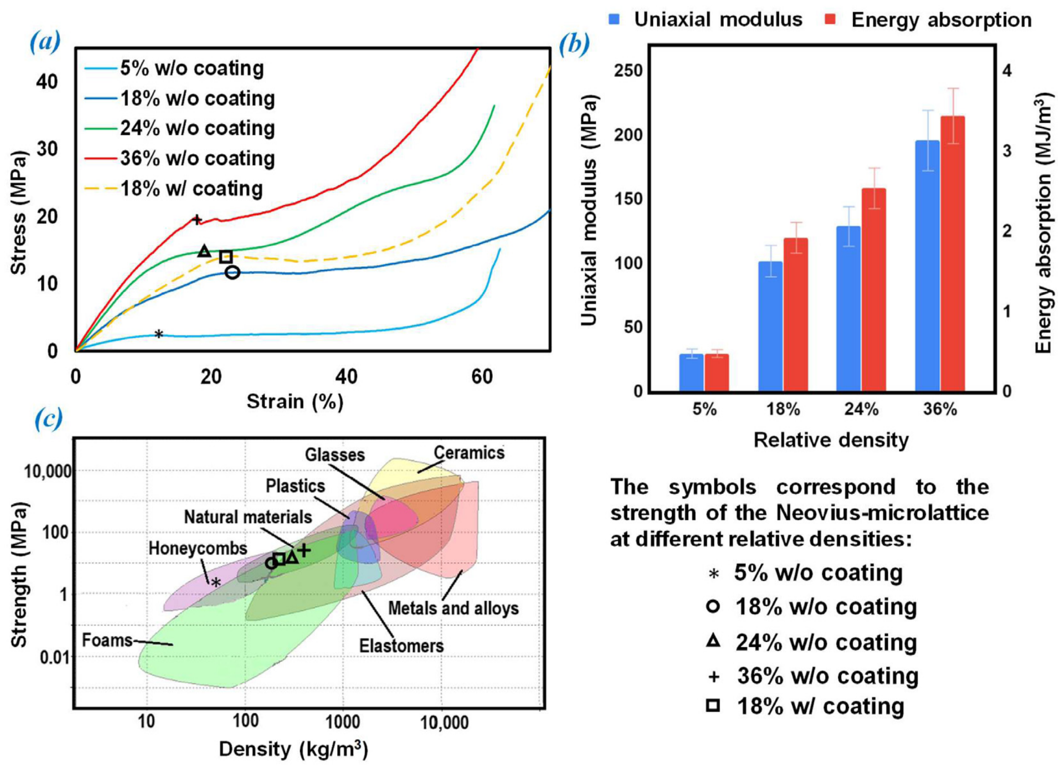

Fig. 4. Stress–strain curves and mechanical properties: (a) stress–strain curves of the Neovius-microlattice at different relative densities, (b) uniaxial stiffness and energy absorption (until 25% applied strain), (c) compressive strength-density Ashby chart with the strengths of the Neovius-microlattice.

during the experiment [8,84]. The theoretical limits discussed above are derived using beam theory and are only applicable to cellular materials with low relative densities [5,35].

The scaling laws of the uniaxial stiffness E, energy absorption EA, and strength S are $E = 509_r^{0.95}(\mathrm{MPa})$, $EA = 10.43\rho_r^{1.02}\left(\frac{MJ}{m^3}\right)$, and $S = 71.1\rho_r^{1.13}(\mathrm{MPa})$, respectively. The above scaling laws are deduced from four different relative densities. The scale laws for stiffness and strength of the Neovius-microlattice indicate a relatively stretching-dominated deformation ($n \approx 1$). Also, the strengths of the Neovius-microlattice lie at the upper border of the foam region shown in the Ashby chart (see Fig. 4c), assuming a density of 1.15 g/cm^3 for the base material [85]. Looking at the scaling laws, the strength of the Neovius-lattice obtained here is higher than the strength of the Neovius-lattice obtained in [70]. This can be attributed to the properties of base materials and fabrication settings (including resolution and relative pixel size). The analytical model of closed-cell cellular solids by Gibson and Ashby [5] (see Fig. 5) can be modified to represent sheet-like lattices, and it can help in providing some insights about the scaling laws in sheet-like materials [8]. The mechanical response of closed-cell foams is the sum of four contributions: cell-edge (shown in orange in Fig. 5) bending, cell-face (shown in gray in Fig. 5) stretching and bending, and gas compression. Since sheet-like lattices are not sealed, the later contribution vanishes. Then, the Gibson–Ashby model reduces to

$$E = C_1(1-\phi)\rho_r + C_1'\phi^2\rho_r^2 + C_1''(1-\phi)^3\rho_r^2 \tag{1}$$

where C_1, C_1', and C_1'' are constants accounting for geometric factors and modulus of base material. ϕ is the fraction of the solid contained in the cell edges, which is given by

$$\phi = \frac{t^2}{t^2 + bL} \tag{2}$$

where $L \gg t$, $L \gg b$. In the case of sheet-like lattices, $t \approx b$; hence, $\phi \to 0$. This indicates that the second term in equation (1) vanishes. At low relative densities, the third term becomes negligible. Following the same argument (assuming $\phi \to 0$ and removing the effect of gas compression), the effective plastic strength using the Gibson–Ashby [5] model reduces to

$$S = C_5\phi^{3/2}\rho_r^{3/2} + C_5''(1-\phi)\rho_r = C_5''\rho_r \tag{3}$$

where C_5 and C_5'' are constants accounting for the geometric factors and yield strength of the base material. Thus, the modulus and plastic strength of sheet-like materials scale linearly with the relative density, which agrees with the experimental results.

Fig. 6 portrays a comparison between the uniaxial modulus and strength obtained experimentally and computationally. The difference error in the case of the uniaxial modulus ranges from 12%–50%, while it ranges from 18%–55% in the case of the strength. This discrepancy between the FEA and experimental results can be attributed to many factors. To mention a few, the FEA results are obtained assuming periodic boundary conditions, where an infinite number of cells is assumed, while the experimental results are based on a finite number of unit cells [70,86]. Also, the finite element model is calibrated by testing bulk columns of the base material following the ASTM D695-15 standard. For a better calibration, one needs to consider different modes of loadings for the base material, such as uniaxial tension, biaxial loading, triaxial loading, and/or shear loading [87]. Other sources of discrepancy are the fabrication settings (such as laser intensity and writing speed), environmental factors (such as humidity and temperature), and aging of the photoresist or the laser source [88]. Such factors may alter the end relative density of the fabricated material, compared to the CAD relative density, and influence the mechanical properties in terms of uniformity, anisotropy, and other factors.

The mechanical properties of the Neovius-microlattice can be enhanced by coating the polymeric lattice with ceramic. To study the effect of the coating, the Neovius-microlattice with a relative

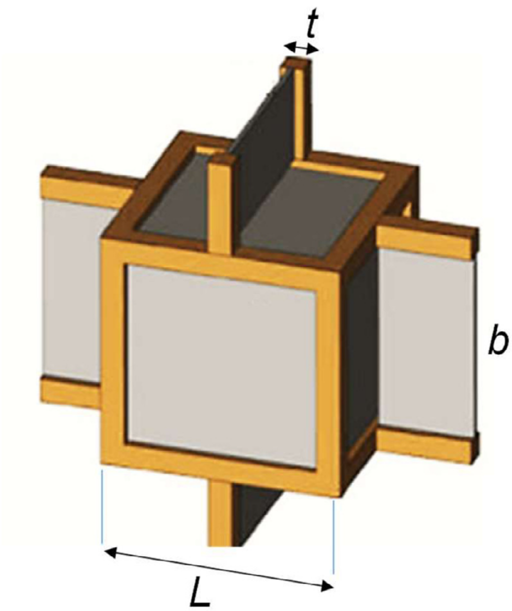

Fig. 5. Gibson–Ashby model for idealized closed cell foams.

density of 18% is coated with alumina Al_2O_3 layer of 10 nm estimated thickness, yielding a ceramic-polymer architectured composite with two continuous phases. In Fig. 4a, the dashed line represents the stress–strain curve of the coated Neovius-microlattice. Such a conformal Al_2O_3coating of the Neovius-microlattice increases its strength by 21%. This significant increase in strength might be attributed to two reasons. The first reason is that the strength of the basic polymer itself is increased due to baking/heating throughout the coating process, as thoroughly discussed in the work of Schroer et al. [33]. They argued that the increase in the polymer strength is related to thermally induced cross-linking of the polymer chains.

Another factor that helps to achieve high strength values is the strengthening mechanism of ceramic occurring at the nano-scale scale. It has been stated that the strength of an ultrathin coating approaches the theoretical strength of Al_2O_3 [29,42]. Ceramic materials usually do not experience plastic flaws at the crack tip, and this leads to low toughness and failure at stresses lower than the yield strength of ceramic materials [34]. Based on Griffith's law, the fracture strength σ_f of a material is given by

$$\sigma_f = \frac{K_c}{Y\sqrt{a}} \quad (4)$$

where K_c is a material constant (fracture toughness), Y is a numerical constant, and a is the size of material's largest crack. Natural materials such as bone and enamel contain mineral (ceramic) platelets a few nanometers thick to form materials with enhanced strength and toughness [26,89]. Having ultrathin coating layer makes a to be in the same order as the coating thickness t. Thus, thin enough ceramic layer might achieve strengths close to the theoretical strength. Bauer et al. [29] concluded that the strength of Al_2O_3 layers between 10 and 50 nm is about 5 GPa, which is around 10 times higher than the strength of the bulk alumina. For the Neovius-microlattice, the polymeric core leads to a tougher material and resists local (in-plane) buckling of the cells, while the alumina coating helps carry the tensile and compressive loadings spread throughout the microlattice.

For $SR = 1$, in-plane (local) buckling and plastic yielding take place, while the out-of-plane (global) buckling is not observed. Next, we discuss the local and global buckling of the Neovius-microlattices having $SR > 1$. Three different SR's are considered: $SR = 2$, $SR = 4$, and $SR = 8$. The deformation modes for the case of $SR = 2$ are like those of $SR = 1$; global buckling does not occur while local buckling and plastic yielding are observed. Increasing the SR further changes the in-plane instability to out-of-plane instability, as depicted in Fig. 7. The local buckling is mainly controlled by the cell-size-to-sheet-thickness ratio $SR_{cell} = l/t$ (Figs. 2a and 2c), while the global instability is primarily governed by $SR = H/T$. Increasing either of them decreases the critical buckling load causing the corresponding instability mechanism [5,61].

Also, the global buckling of the Neovius-lattice is studied using FEA (linear eigen buckling [59,61,70,81,90]). A compressive force is applied perpendicular to the top face with zero displacements in the lateral directions, the sides are traction-free, while the bottom face is fixed (zero displacements in the three Cartesian directions). For more details on the distinction between local and global buckling of architectured materials using linear eigen buckling analysis, readers are referred elsewhere [59,61,90]. Mesh sensitivity analysis was performed to ensure that the obtained results are mesh independent. Fig. 7a–b and 7 d–e illustrate the global buckling of the Neovius-lattice for $SR = 8$ and $SR = 4$, respectively. The global instability modes obtained from linear eigen buckling analysis are in good agreement with experimental results, while the critical buckling loads obtained from the FEA are within 10% error. Also, we discuss the effect of ceramic coating on the mechanical response of the Neovius-microlattice with high SR. Figs. 7b and 5c show the deformations of uncoated and coated Neovius-microlattices, respectively. Initially, out-of-plane (global) buckling is observed in both cases. For the uncoated microlattice, higher strains result in highly bent lattice without the observance of any visible fractures. On the other hand, the

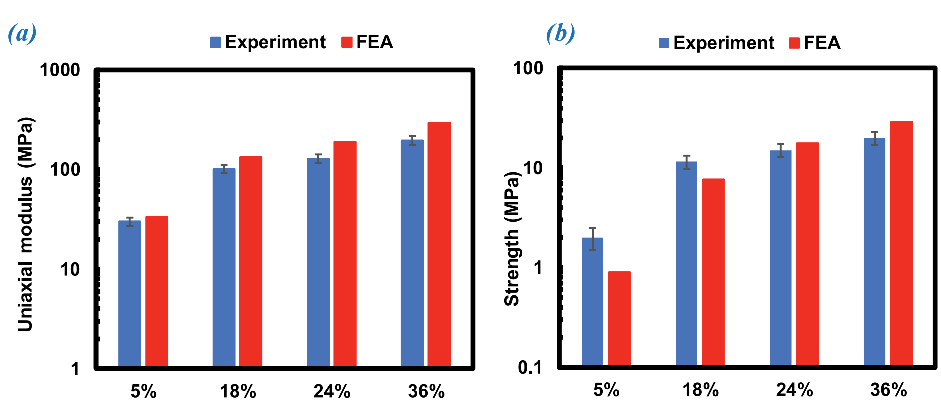

Fig. 6. Comparison between finite element analysis (FEA) results and experimental results: (a) uniaxial modulus, (b) compressive strength. A base-10 log scale is used for the y-axis.

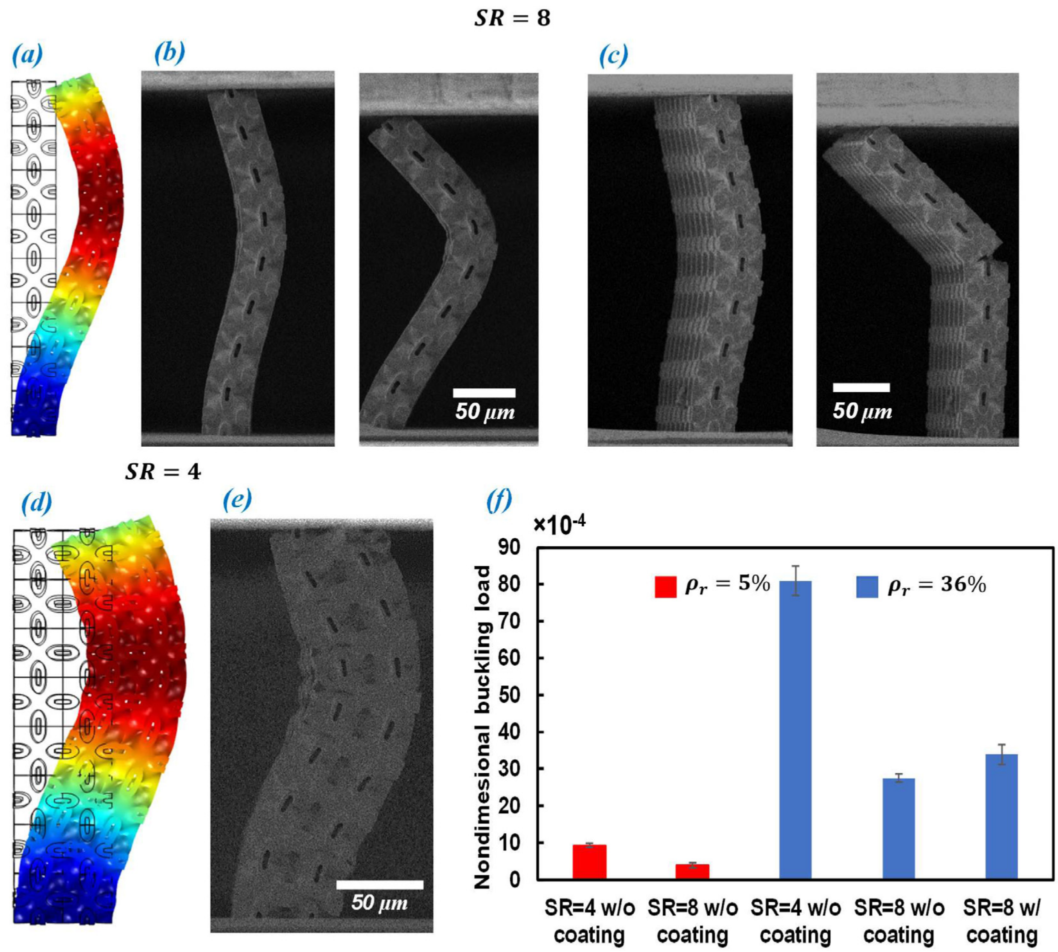

Fig. 7. Buckling analysis of the Neovius-microlattices (ρ_r = 36%) with different slenderness ratio *SR*: (a) total displacement of $SR = 8$ obtained from the linear eigen buckling (b) buckled Neovius-microlattice without coating ($SR = 8$) at two different strains, (c) buckling/fracturing of microlattice coated with alumina ($SR = 8$) at two different strains, (d) total displacement of $SR = 4$ obtained from the linear eigen buckling analysis, (e) buckled Neovius-microlattice ($SR = 4$), (f) nondimensional buckling load of the Neovius-microlattices with different slenderness ratios and relative density.

coated microlattice experiences fracture in the middle of the microlattice height. As the Neovius-microlattice with $SR = 2$ does not buckle globally, its modulus and strength are comparable to those of the Neovius-microlattice with $SR = 1$, as shown in Fig. 4.

Fig. 7f represents the nondimensional buckling load of the Neovius-microlattice possessing two relative densities ($\rho_r = 5\%$ and $\rho_r = 36\%$) and two slenderness ratios ($SR = 4$ and $SR = 8$). The nondimensional buckling load $\overline{N}_{cr}$ [61,91] is defined as

$$\overline{N}_{cr} = \frac{\hat{N}H^2}{E_s W^3} \tag{5}$$

where $\hat{N}$ is the in-plane compressive load per unit width W. The nondimensional buckling load increases with the increase of the relative density and decrease of the slenderness ratio. Also, the nondimensional buckling load could be increased by coating the microarchitectured lattice. It would be interesting to compare the nondimensional buckling loads of the Neovius-microlattice with other 3D microlattices. Additionally, the buckling load of the Neovius-microlattice ($\rho_r = 36\%$ and $SR = 8$) is increased by 23% when coating it with an alumina layer with 10 nm estimated thickness, as shown in Fig. 7f. This significant increase is due to two factors: the baking of the base polymer and size effect in the ceramic layer, as discussed earlier. The distinction between out-of-plane (global) and in-plane (local) buckling could be very useful in studies of other architectured materials, modeling of multiscale problems [47,92], and developing new hierarchical materials [38,93,94] with multilength-scale building blocks. For instance, designing hierarchical materials such that materials at lower scales deform locally (fracture, plastic yielding, or in-plane buckling) rather than globally (out-of-plane buckling) may lead to materials with overall enhanced responses.

4. Conclusions

In summary, we discussed the design, fabrication, testing, and modeling of the Neovius-microlattice. The results of this study show that the Neovius-microlattice achieves outstanding mechanical properties under compressive loading due to the continuous nature of the Neovius-microlattice. The mechanical properties (under compression) of the Neovius-microlattice are further enhanced by coating the microlattice with alumina exploiting the size effect phenomenon accompanying ultrathin ceramic layers. Additionally, we distinguished between out-of-plane (global) and in-plane (local) buckling. At the local level, the Neovius-microlattice experiences in-plane buckling and plastic yielding, where the in-plane buckling occurs partially (at the openings of the Neovius-lattice). In other words, the cell does not lose its load-bearing capability even when local buckling takes place. Also, the absence of joints reduces the stress concentration effect. When the slenderness ratio is increased, out-of-plane buckling starts to be the governing failure mechanism. This study shows that sheet-like materials have promising potential to be utilized as microarchitected materials.

Declaration of competing interest

The authors declare that they have no known competing financial interests or personal relationships that could have appeared to influence the work reported in this paper.

Acknowledgments

The fabrication of the specimens was carried out in the Materials Research Laboratory Central Research Facilities, University of Illinois. The experimental testing was carried out in the Beckman Institute of Science and Technology, University of Illinois. The authors would like to thank Scott J. Robinson and Leilei Yin for technical support. I.J. would like to acknowledge the National Science Foundation grant MOMS-1926353 and the ZJU-UIUC Institute Research Program Funding .

References

[1] N.A. Fleck, V.S. Deshpande, M.F. Ashby, Micro-architectured materials: past, present and future, Proc. R. Soc. Ser. A Math. Phys. Eng. Sci. 466 (2010) 2495–2516.
[2] M.F. Ashby, H. Shercliff, D. Cebon, Materials: Engineering, Science, Processing and Design, Butterworth-Heinemann, 2018.
[3] M.G. Rashed, M. Ashraf, R.A.W. Mines, P.J. Hazell, Metallic microlattice materials: A current state of the art on manufacturing, mechanical properties and applications, Mater. Des. 95 (2016) 518–533.
[4] J. Xiong, R. Mines, R. Ghosh, A. Vaziri, L. Ma, A. Ohrndorf, H. Christ, L. Wu, Advanced micro-lattice materials, Adv. Energy Mater. 17 (2015) 1253–1264.
[5] L.J. Gibson, M.F. Ashby, Cellular Solids: Structure and Properties, Cambridge University Press, 1999.
[6] L. Valdevit, A.J. Jacobsen, J.R. Greer, W.B. Carter, Protocols for the optimal design of multi-functional cellular structures: from hypersonics to micro-architected materials, J. Am. Ceram. Soc. 94 (2011) s15–s34.
[7] S.N. Khaderi, V.S. Deshpande, N.A. Fleck, The stiffness and strength of the gyroid lattice, Int. J. Solids Struct. 51 (2014) 3866–3877.
[8] O. Al-Ketan, R. Rezgui, R. Rowshan, H. Du, N.X. Fang, R.K. Abu Al-Rub, Microarchitected stretching-dominated mechanical metamaterials with minimal surface topologies, Adv. Energy Mater. 20 (2018) 1800029.
[9] V.F. Chernow, H. Alaeian, J.A. Dionne, J.R. Greer, Polymer lattices as mechanically tunable 3-dimensional photonic crystals operating in the infrared, Appl. Phys. Lett. 107 (2015) 101905.
[10] X. Xia, C.V. Di Leo, X.W. Gu, J.R. Greer, In situ lithiation–delithiation of mechanically robust Cu–Si core–shell nanolattices in a scanning electron microscope, ACS Energy Lett. 1 (2016) 492–499.
[11] T.A. Schaedler, A.J. Jacobsen, A. Torrents, A.E. Sorensen, J. Lian, J.R. Greer, L. Valdevit, W.B. Carter, Ultralight metallic microlattices, Science 334 (2011) 962–965.
[12] D.W. Abueidda, P. Karimi, J.-M. Jin, N.A. Sobh, I.M. Jasiuk, M. Ostoja-Starzewski, Shielding effectiveness and bandgaps of interpenetrating phase composites based on the Schwarz primitive surface, J. Appl. Phys. 124 (2018) 175102.
[13] T. Juarez, A. Schroer, R. Schwaiger, A.M. Hodge, Evaluating sputter deposited metal coatings on 3D printed polymer micro-truss structures, Mater. Des. 140 (2018) 442–450.
[14] A.G. Izard, L. Valdevit, Magnetoelastic metamaterials for energy dissipation and wave filtering, Adv. Energy Mater. 22 (2019) 190101.
[15] S.C. Han, K. Kang, Another stretching-dominated micro-architectured material, shellular, Mater. Today 31 (2019) 31–38.
[16] J. Paulose, A.S. Meeussen, V. Vitelli, Selective buckling via states of self-stress in topological metamaterials, Proc. Natl. Acad. Sci. 112 (2015) 7639–7644.
[17] S.S. Injeti, C. Daraio, K. Bhattacharya, Metamaterials with engineered failure load and stiffness, Proc. Natl. Acad. Sci. 116 (2019) 23960–23965.
[18] M. Ruzzene, F. Scarpa, Directional and band-gap behavior of periodic auxetic lattices, Phys. Status Solidi B 242 (2005) 665–680.
[19] J. Schiøtz, F.D. Di Tolla, K.W. Jacobsen, Softening of nanocrystalline metals at very small grain sizes, Nature 391 (1998) 561–563.
[20] X. Zheng, H. Lee, T.H. Weisgraber, M. Shusteff, J. DeOtte, E.B. Duoss, J.D. Kuntz, M.M. Biener, Q. Ge, J.A. Jackson, Ultralight, ultrastiff mechanical metamaterials, Science 344 (2014) 1373–1377.
[21] G.Z. Voyiadjis, R.K. Abu Al-Rub, Gradient plasticity theory with a variable length scale parameter, Int. J. Solids Struct. 42 (2005) 3998–4029.
[22] J.S. Stölken, A.G. Evans, A microbend test method for measuring the plasticity length scale, Acta Mater. 46 (1998) 5109–5115.
[23] P. Shrotriya, S.M. Allameh, J. Lou, T. Buchheit, W.O. Soboyejo, On the measurement of the plasticity length scale parameter in LIGA nickel foils, Mech. Mater. 35 (2003) 233–243.
[24] M.A. Haque, M.T.A. Saif, Strain gradient effect in nanoscale thin films, Acta Mater. 51 (2003) 3053–3061.
[25] A. Torrents, T.A. Schaedler, A.J. Jacobsen, W.B. Carter, L. Valdevit, Characterization of nickel-based microlattice materials with structural hierarchy from the nanometer to the millimeter scale, Acta Mater. 60 (2012) 3511–3523.
[26] S. Weiner, H.D. Wagner, The material bone: structure-mechanical function relations, Annu. Rev. Mater. Sci. 28 (1998) 271–298.
[27] D. Jang, L.R. Meza, F. Greer, J.R. Greer, Fabrication and deformation of three-dimensional hollow ceramic nanostructures, Nature Mater. 12 (2013) 893–898.
[28] J.T. Muth, P.G. Dixon, L. Woish, L.J. Gibson, J.A. Lewis, Architected cellular ceramics with tailored stiffness via direct foam writing, Proc. Natl. Acad. Sci. 114 (2017) 1832–1837.
[29] J. Bauer, A. Schroer, R. Schwaiger, I. Tesari, C. Lange, L. Valdevit, O. Kraft, Push-to-pull tensile testing of ultra-strong nanoscale ceramic–polymer composites made by additive manufacturing, Extreme Mech. Lett. 3 (2015) 105–112.
[30] J. Bauer, C. Crook, A. Guell Izard, Z.C. Eckel, N. Ruvalcaba, T.A. Schaedler, L. Valdevit, Additive manufacturing of ductile, ultrastrong polymer-derived nanoceramics, Matter 1 (2019) 1547–1556.
[31] D.W. Abueidda, F.A. Sabet, I.M. Jasiuk, Modeling of stiffness and strength of bone at nanoscale, J. Biomech. Eng. 139 (2017) 51006.
[32] L.J. Gibson, Biomechanics of cellular solids, J. Biomech. 38 (2005) 377–399.
[33] A. Schroer, J. Bauer, R. Schwaiger, O. Kraft, Optimizing the mechanical properties of polymer resists for strong and light-weight micro-truss structures, Extreme Mech. Lett. 8 (2016) 283–291.
[34] L. Valdevit, J. Bauer, Chapter 13.1 - fabrication of 3D micro-architected/nano-architected materials, in: T. Baldacchini (Ed.), Three-Dimensional Microfabrication using Two-Photon Polymerization, William Andrew Publishing, Oxford, 2016, pp. 345–373, http://dx.doi.org/10.1016/B978-0-323-35321-2.00018-2.
[35] X. Zhang, Y. Wang, B. Ding, X. Li, Design, fabrication, and mechanics of 3D micro-/nanolattices, Small (2019) 1902842.
[36] R. Liontas, J.R. Greer, 3D Nano-architected metallic glass: Size effect suppresses catastrophic failure, Acta Mater. 133 (2017) 393–407.
[37] R. Schwaiger, L.R. Meza, X. Li, The extreme mechanics of micro- and nanoarchitected materials, MRS Bull. 44 (2019) 758–765.
[38] L.R. Meza, A.J. Zelhofer, N. Clarke, A.J. Mateos, D.M. Kochmann, J.R. Greer, Resilient 3D hierarchical architected metamaterials, Proc. Natl. Acad. Sci. 112 (2015) 11502–11507.
[39] J. Bauer, A. Schroer, R. Schwaiger, O. Kraft, Approaching theoretical strength in glassy carbon nanolattices, Nature Mater. 15 (2016) 438–443.
[40] M. Deubel, G. Von Freymann, M. Wegener, S. Pereira, K. Busch, C.M. Soukoulis, Direct laser writing of three-dimensional photonic-crystal templates for telecommunications, Nature Mater. 3 (2004) 444–447.
[41] L.R. Meza, G.P. Phlipot, C.M. Portela, A. Maggi, L.C. Montemayor, A. Comella, D.M. Kochmann, J.R. Greer, Reexamining the mechanical property space of three-dimensional lattice architectures, Acta Mater. 140 (2017) 424–432.
[42] J. Bauer, S. Hengsbach, I. Tesari, R. Schwaiger, O. Kraft, High-strength cellular ceramic composites with 3D microarchitecture, Proc. Natl. Acad. Sci. 111 (2014) 2453–2458.
[43] L.R. Meza, S. Das, J.R. Greer, Strong, lightweight, and recoverable three-dimensional ceramic nanolattices, Science 345 (2014) 1322–1326.
[44] S.-W. Lee, M. Jafary-Zadeh, D.Z. Chen, Y.-W. Zhang, J.R. Greer, Size effect suppresses brittle failure in hollow Cu60Zr40 metallic glass nanolattices deformed at cryogenic temperatures, Nano Lett. 15 (2015) 5673–5681.
[45] X. Zhang, J. Yao, B. Liu, J. Yan, L. Lu, Y. Li, H. Gao, X. Li, Three-dimensional high-entropy alloy–polymer composite nanolattices that overcome the strength–recoverability trade-off, Nano Lett. 18 (2018) 4247–4256.
[46] X. Zhang, A. Vyatskikh, H. Gao, J.R. Greer, X. Li, Lightweight, flaw-tolerant, and ultrastrong nanoarchitected carbon, Proc. Natl. Acad. Sci. 116 (2019) 6665–6672.
[47] X. Zheng, W. Smith, J. Jackson, B. Moran, H. Cui, D. Chen, J. Ye, N. Fang, N. Rodriguez, T. Weisgraber, Multiscale metallic metamaterials, Nature Mater. 15 (2016) 1100–1106.
[48] C. Sun, N. Fang, D.M. Wu, X. Zhang, Projection micro-stereolithography using digital micro-mirror dynamic mask, Sensors Actuators A 121 (2005) 113–120.
[49] J.U. Surjadi, L. Gao, H. Du, X. Li, X. Xiong, N.X. Fang, Y. Lu, Mechanical metamaterials and their engineering applications, Adv. Energy Mater. 21 (2019) 1800864.
[50] A.J. Jacobsen, W. Barvosa-Carter, S. Nutt, Micro-scale truss structures formed from self-propagating photopolymer waveguides, Adv. Mater. 19 (2007) 3892–3896.
[51] A.J. Jacobsen, W. Barvosa-Carter, S. Nutt, Compression behavior of micro-scale truss structures formed from self-propagating polymer waveguides, Acta Mater. 55 (2007) 6724–6733.

[52] J.R. Tumbleston, D. Shirvanyants, N. Ermoshkin, R. Janusziewicz, A.R. Johnson, D. Kelly, K. Chen, R. Pinschmidt, J.P. Rolland, A. Ermoshkin, Continuous liquid interface production of 3D objects, Science 347 (2015) 1349–1352.
[53] M.A. Haque, M.T.A. Saif, In-situ tensile testing of nano-scale specimens in SEM and TEM, Exp. Mech. 42 (2002) 123–128.
[54] D.J. Stokes, A.M. Donald, In situ mechanical testing of dry and hydrated breadcrumb in the environmental scanning electron microscope (ESEM), J. Mater. Sci. 35 (2000) 599–607.
[55] H.T. Vo, A. Reichardt, D. Frazer, N. Bailey, P. Chou, P. Hosemann, In situ micro-tensile testing on proton beam-irradiated stainless steel, J. Nucl. Mater. 493 (2017) 336–342.
[56] J. Zhu, X. Zhang, H. Luo, E. Sahraei, Investigation of the deformation mechanisms of lithium-ion battery components using in-situ micro tests, Appl. Energy 224 (2018) 251–266.
[57] J.T.B. Overvelde, S. Shan, K. Bertoldi, Compaction through buckling in 2d periodic, soft and porous structures: effect of pore shape, Adv. Mater. 24 (2012) 2337–2342.
[58] Y. He, S. Guo, Z. Liu, K.M. Liew, Pattern transformation of thermo-responsive shape memory polymer periodic cellular structures, Int. J. Solids Struct. 71 (2015) 194–205.
[59] M.E. Rackliffe, D.W. Jensen, W.K. Lucas, Local and global buckling of ultra-lightweight IsoTruss® structures, Compos. Sci. Technol. 66 (2006) 283–288.
[60] M. Kucewicz, P. Baranowski, J. Małachowski, A. Popławski, P. Płatek, Modelling, and characterization of 3D printed cellular structures, Mater. Des. 142 (2018) 177–189.
[61] H. Niknam, A.H. Akbarzadeh, In-plane and out-of-plane buckling of architected cellular plates: Numerical and experimental study, Compos. Struct. 206 (2018) 739–749.
[62] Y. He, Y. Zhou, Z. Liu, K.M. Liew, Buckling and pattern transformation of modified periodic lattice structures, Extreme Mech. Lett. 22 (2018) 112–121.
[63] M. Afshar, A.P. Anaraki, H. Montazerian, J. Kadkhodapour, Additive manufacturing and mechanical characterization of graded porosity scaffolds designed based on triply periodic minimal surface architectures, J. Mech. Behav. Biomed. Mater. 62 (2016) 481–494.
[64] K. Michielsen, D.G. Stavenga, Gyroid cuticular structures in butterfly wing scales: biological photonic crystals, J. R. Soc. Interface 5 (2007) 85–94.
[65] J.W. Galusha, L.R. Richey, J.S. Gardner, J.N. Cha, M.H. Bartl, Discovery of a diamond-based photonic crystal structure in beetle scales, Phys. Rev. E 77 (2008) 50904.
[66] D.W. Abueidda, A.S. Dalaq, R.K. Abu Al-Rub, H.A. Younes, Finite element predictions of effective multifunctional properties of interpenetrating phase composites with novel triply periodic solid shell architectured reinforcements, Int. J. Mech. Sci. 92 (2015) 80–89.
[67] O. Al-Ketan, M.A. Assad, R.K. Abu Al-Rub, Mechanical properties of periodic interpenetrating phase composites with novel architected microstructures, Compos. Struct. 176 (2017) 9–19.
[68] D.W. Abueidda, M. Elhebeary, C.-S.A. Shiang, S. Pang, R.K. Abu Al-Rub, I.M. Jasiuk, Mechanical properties of 3D printed polymeric gyroid cellular structures: Experimental and finite element study, Mater. Des. 165 (2019) 107597.
[69] D.W. Abueidda, I. Jasiuk, N.A. Sobh, Acoustic band gaps and elastic stiffness of PMMA cellular solids based on triply periodic minimal surfaces, Mater. Des. 145 (2018) 20–27.
[70] D.W. Abueidda, M. Bakir, R.K. Abu Al-Rub, J.S. Bergström, N.A. Sobh, I. Jasiuk, Mechanical properties of 3D printed polymeric cellular materials with triply periodic minimal surface architectures, Mater. Des. 122 (2017) 255–267.
[71] O. Al-Ketan, R. Rowshan, R.K. Abu Al-Rub, Topology-mechanical property relationship of 3D printed strut, skeletal, and sheet based periodic metallic cellular materials, Addit. Manuf. 19 (2018) 167–183.
[72] J. Feng, J. Fu, C. Shang, Z. Lin, B. Li, Sandwich panel design and performance optimization based on triply periodic minimal surfaces, Comput. Aided Des. 115 (2019) 307–322.
[73] S.C. Han, J.W. Lee, K. Kang, A new type of low density material: Shellular, Adv. Mater. 27 (2015) 5506–5511.
[74] K.A. Khan, R.K. Abu Al-Rub, Viscoelastic properties of architected foams based on the Schoen IWP triply periodic minimal surface, Mech. Adv. Mater. Struct. (2018) 1–14.
[75] I. Maskery, L. Sturm, A.O. Aremu, A. Panesar, C.B. Williams, C.J. Tuck, R.D. Wildman, I.A. Ashcroft, R.J.M. Hague, Insights into the mechanical properties of several triply periodic minimal surface lattice structures made by polymer additive manufacturing, Polymer 152 (2018) 62–71.
[76] W. Lee, D.-Y. Kang, J. Song, J.H. Moon, D. Kim, Controlled unusual stiffness of mechanical metamaterials, Sci. Rep. 6 (2016) 20312.
[77] A.-I. Bunea, M.H. Jakobsen, E. Engay, A.R. Bañas, J. Glückstad, Optimization of 3D-printed microstructures for investigating the properties of the mucus biobarrier, Micro Nano Eng. 2 (2019) 41–47.
[78] S.M. George, Atomic layer deposition: an overview, Chem. Rev. 110 (2009) 111–131.
[79] J.X. Liu, S.C. Deng, J. Zhang, N.G. Liang, Lattice type of fracture model for concrete, Theor. Appl. Fract. Mech. 48 (2007) 269–284.
[80] J.C. Simo, T.J.R. Hughes, Computational Inelasticity, Springer Science & Business Media, 2006.
[81] L. Valdevit, S.W. Godfrey, T.A. Schaedler, A.J. Jacobsen, W.B. Carter, Compressive strength of hollow microlattices: Experimental characterization, modeling, and optimal design, J. Mater. Res. 28 (2013) 2461–2473.
[82] Z. Vangelatos, V. Melissinaki, M. Farsari, K. Komvopoulos, C. Grigoropoulos, Intertwined microlattices greatly enhance the performance of mechanical metamaterials, Math. Mech. Solids 24 (2019) 2636–2648.
[83] J. Bauer, A. Schroer, R. Schwaiger, O. Kraft, The impact of size and loading direction on the strength of architected lattice materials, Adv. Energy Mater. 18 (2016) 1537–1543.
[84] J. Bauer, L.R. Meza, T.A. Schaedler, R. Schwaiger, X. Zheng, L. Valdevit, Nanolattices: an emerging class of mechanical metamaterials, Adv. Mater. 29 (2017) 1701850.
[85] T. Frenzel, M. Kadic, M. Wegener, Three-dimensional mechanical metamaterials with a twist, Science 358 (2017) 1072–1074.
[86] D.W. Abueidda, R.K. Abu Al-Rub, A.S. Dalaq, D.-W. Lee, K.A. Khan, I. Jasiuk, Effective conductivities and elastic moduli of novel foams with triply periodic minimal surfaces, Mech. Mater. 95 (2016) 102–115.
[87] K. Upadhyay, A. Bhattacharyya, G. Subhash, D.E. Spearot, Quasi-static and high strain rate simple shear characterization of soft polymers, Exp. Mech. 59 (2019) 733–747.
[88] L. Valdevit, J. Bauer, Chapter 13.1 - Fabrication of 3D micro-/nanoarchitected materials, in: T. Baldacchini (Ed.), Micro and Nano Technologies, Three-Dimensional Microfabrication Using Two-Photon Polymerization, William Andrew Publishing, 2020, pp. 541–576, http://dx.doi.org/10.1016/B978-0-12-817827-0.00013-8.
[89] H.P. Schwarcz, D. Abueidda, I. Jasiuk, The ultrastructure of bone and its relevance to mechanical properties, Front. Phys. 5 (2017) 39–51.
[90] Q. Sui, H. Fan, C. Lai, Failure analysis of 1D lattice truss composite structure in uniaxial compression, Compos. Sci. Technol. 118 (2015) 207–216.
[91] J.N. Reddy, Mechanics of Laminated Composite Plates and Shells: Theory and Analysis, CRC press, 2003.
[92] K. Matouš, M.G.D. Geers, V.G. Kouznetsova, A. Gillman, A review of predictive nonlinear theories for multiscale modeling of heterogeneous materials, J. Comput. Phys. 330 (2017) 192–220.
[93] Y. Xu, Chapter 19 - Hierarchical materials, in: Modern Inorganic Synthetic Chemistry, Elsevier, Amsterdam, 2017, pp. 545–574, http://dx.doi.org/10.1016/B978-0-444-63591-4.00019-7.
[94] S. Yin, H. Chen, J. Li, T.X. Yu, J. Xu, Effects of architecture level on mechanical properties of hierarchical lattice materials, Int. J. Mech. Sci. 157–158 (2019) 282–292.